Time-domain simulation of a dissipative reed instrument

Alexis Thibault, Juliette Chabassier

TIME-DOMAIN SIMULATION OF A DISSIPATIVE REED INSTRUMENT

Alexis Thibault[1] **Juliette Chabassier**[1]

[1] Inria Bordeaux Sud-Ouest – Magique-3D team – Université de Pau et des Pays de l'Adour

alexis.thibault@inria.fr

ABSTRACT

Sound synthesis of reed wind instruments requires special care to ensure numerical stability and accuracy of the time-domain simulation. Energy-based methods have proven very efficient for this purpose, where the instrument model is split into several sub-systems which exchange and dissipate a numerical analog of the physical energy. A wide range of reed, propagation, tone hole and radiation models may thus be coupled. Space discretization is performed using 1D spectral finite elements, offering an affordable, flexible and more accurate alternative to finite differences for computing propagation of the acoustic waves along the instrument's bore, and energy-consistent time-stepping schemes are used for numerical integration of the equations. Whenever implicit couplings are used to ensure energy consistency, algorithmic tricks allow us to update all the unknowns explicitly via algebraic elimination, such that in the end, no matrix inversion is required. We will present some of the models and numerical schemes implemented in our open-source software OpenWInD (openwind.gitlabpages.inria.fr/web), including a new model for approximating losses due to viscothermal boundary layers in the time domain. Simulation code will be made available in the toolbox OpenWInD under GPLv3.

1. INTRODUCTION

This work is part of the OpenWInD project, which aims at making up-to-date models of wind instrument acoustics widely available to research teams and instrument makers. All the results of this paper have been obtained using OpenWInD toolbox. The latest public version can be downloaded under GPLv3 licence on our website [1].

Time-domain simulation of a wind instrument has been addressed in various ways, many of which rely on a simplified version of a resonator, such as digital waveguides [2], or impedance-based methods [3]. The approach presented thereafter aims for high numerical precision; for this reason it is based on the direct simulation of the 1D partial differential equation of wave propagation in a variable section pipe . Such simulation has been successfully performed with finite-differences time-domain methods [4]. The current spatial discretization generalizes this approach to high order by using 1D spectral finite elements. This variational framework is well suited to the inclusion of time-varying and non-linear effects such as tone holes that can be opened and closed continuously, or a lumped reed. To ensure stability, the models must be chosen appropriately so that each verifies an energy balance equation. Through appropriate time-stepping schemes, discrete energy balance equations are then preserved at the numerical level.

Section 2 presents the physical models used for acoustic propagation, radiation, tone holes, and reed. Section 3 explains the space- and time-discretizations. Finally, section 4 gives an example of use of OpenWInD on a real bassoon.

2. PHYSICAL MODELS

2.1 Acoustic propagation

The classical horn equations describing plane wave propagation in an axisymmetric lossless pipe of length L with varying section $S(x)$ are written as [5]:

$$\begin{cases} \dfrac{\rho}{S}\partial_t v + \partial_x p = 0, \quad x \in [0, L] & \text{(1a)} \\ \dfrac{S}{\rho c^2}\partial_t p + \partial_x v = 0, \quad x \in [0, L], & \text{(1b)} \end{cases}$$

where ρ is the quiescent density, c is the acoustic celerity, and the unknowns $p(x,t)$ and $u(x,t)$ represent respectively the pressure and flow through each cross-section. System (1) must be complemented by boundary conditions relating $p(0,t)$ with the flow exiting the pipe $-v(0,t)$, and similarly $p(L,t)$ with $v(L,t)$: these are described below.

System (1) always verifies the following energy balance:

$$\frac{d\mathcal{E}}{dt} = v(0,t)p(0,t) - v(L,t)p(L,t) - Q(t), \quad (2)$$

$$\text{where} \quad \mathcal{E} = \frac{1}{2}\int_0^L \frac{\rho}{S}v^2 dx + \frac{1}{2}\int_0^L \frac{S}{\rho c^2}p^2 dx, \quad (3)$$

and the dissipation term is $Q(t) = 0$, signifying that variation of energy is only due to work exchanged at the ends of the tube.

2.2 Propagation with viscothermal losses

Energy losses due to viscosity and thermal effects can be expressed in the harmonic domain as non-rational functions of frequency [6]. In order to approximate the corresponding pseudo-differential operators, $2N + 1$ auxiliary

variables $v_i(x,t)$, $p_0(x,t)$, $p_i(x,t)$ are introduced [7, 8]:

$$\begin{cases} \frac{\rho}{S}\partial_t v + R_0 v + \sum_{i=1}^N R_i(v - v_i) + \partial_x p = 0, & \text{(4a)} \\ \frac{S}{\rho c^2}\partial_t p + G_0(p - p_0) + \sum_{i=1}^N G_i(p - p_0 - p_i) \\ \qquad\qquad + \partial_x v = 0, & \text{(4b)} \\ L_i \frac{d}{dt} v_i = R_i(v - v_i), \quad \text{for } 1 \le i \le N, & \text{(4c)} \\ C_0 \frac{d}{dt} p_0 = G_0(p - p_0) \\ \qquad + \sum_{i=1}^N G_i(p - p_0 - p_i), & \text{(4d)} \\ C_i \frac{d}{dt} p_i = G_i(p - p_0 - p_i) \quad \text{for } 1 \le i \le N, & \text{(4e)} \end{cases}$$

where the choice of integer N is a trade-off between precision of the approximation and computational cost. The coefficients of this system are defined as

$$\begin{cases} R_0(x) = \frac{\pi\mu}{S(x)^2} a_0, & \text{(5a)} \\ L_i(x) = \frac{\rho}{S(x)} a_i, \; R_i(x) = \frac{\pi\mu}{S(x)^2} \frac{a_i}{b_i}, & \text{(5b)} \\ C_0(x) = \frac{S(x)(\gamma-1)}{\rho c^2}, \; G_0 = \frac{\pi\kappa(\gamma-1)}{\rho^2 c^2 C_P} a_0, & \text{(5c)} \\ C_i(x) = \frac{S(x)(\gamma-1)}{\rho c^2} a_i, \; G_i = \frac{\pi\kappa(\gamma-1)}{\rho^2 c^2 C_P} \frac{a_i}{b_i}, & \text{(5d)} \end{cases}$$

where μ is the viscosity, κ is the thermal conductivity, C_P is the specific heat with constant pressure, and the coefficients a_i and b_i are dimensionless constants obtained from an optimization procedure, see Table 1 for $N \in \{2, 4, 8\}$. The technique from [7] requires to perform several optimizations depending on the physical and geometrical parameters. By contrast, in our formalism a single optimization procedure has been done [8], and the dependence of coefficients (R_i, L_i, C_i, G_i) on physical parameters is explicit.

i	a_i	b_i
0	8	
1	$5.829\,22 \times 10^{-2}$	$2.737\,45 \times 10^{-4}$
2	$2.005\,69 \times 10^{-3}$	$3.284\,31 \times 10^{-7}$

Coefficients for $N = 2$

i	a_i	b_i
0	8	
1	$1.788\,20 \times 10^{-1}$	$4.894\,08 \times 10^{-3}$
2	$2.252\,97 \times 10^{-2}$	$8.061\,16 \times 10^{-5}$
3	$2.957\,06 \times 10^{-3}$	$1.397\,82 \times 10^{-6}$
4	$4.227\,96 \times 10^{-4}$	$2.295\,78 \times 10^{-8}$

Coefficients for $N = 4$

i	a_i	b_i
0	8	
1	$2.098\,23 \times 10^{-1}$	$2.474\,86 \times 10^{-2}$
2	$7.254\,46 \times 10^{-2}$	$2.825\,34 \times 10^{-3}$
3	$2.472\,34 \times 10^{-2}$	$3.304\,86 \times 10^{-4}$
4	$8.482\,65 \times 10^{-3}$	$3.908\,28 \times 10^{-5}$
5	$2.919\,83 \times 10^{-3}$	$4.639\,50 \times 10^{-6}$
6	$1.006\,47 \times 10^{-3}$	$5.516\,88 \times 10^{-7}$
7	$3.505\,10 \times 10^{-4}$	$6.520\,03 \times 10^{-8}$
8	$1.764\,48 \times 10^{-4}$	$5.169\,62 \times 10^{-9}$

Coefficients for $N = 8$

Table 1. Coefficients (a_i, b_i) to use in (5), optimized for radii of 5×10^{-4} m to 0.1 m and frequencies of 20 Hz to 2×10^4 Hz.

Additional terms appear in the expression of the energy (3), and the dissipation term $Q(t)$ becomes positive:

$$\mathcal{E} = \frac{1}{2}\int_\Omega \Big[\tfrac{\rho}{S} v^2 + \tfrac{S}{\rho c^2} p^2 + C_0 p_0^2 + \sum_{i=1}^N C_i p_i^2 + \sum_{i=1}^N L_i v_i^2 \Big], \quad (6)$$

$$Q(t) = \int_\Omega \Big[R_0 v^2 + \sum_{i=1}^N R_i (v - v_i)^2 + G_0 (p - p_0)^2 + \sum_{i=1}^N G_i (p - p_0 - p_i)^2 \Big] \ge 0 \quad (7)$$

In the following, the equations for lossless propagation are assumed, but all techniques can also be applied to the model with losses, as described in [8].

2.3 Radiation impedance

The relation between pressure and flow at the radiating end of an instrument is often expressed in the Fourier domain through a radiation impedance [6]. The primary model used in OpenWInD is (using convention $e^{j\omega t}$ for the Fourier transform):

$$\frac{\hat{p}(L,\omega)}{\hat{v}(L,\omega)} = Z_R = Z_c \frac{j\omega}{\alpha + j\omega\beta}, \quad (8)$$

where $Z_c = \frac{\rho c}{S}$ is the characteristic impedance at the end of the pipe, and the two parameters α and β can be chosen to fit various radiation models. This leads to time-domain system:

$$Z_c \frac{dv}{dt} = \alpha p + \beta \frac{dp}{dt} \quad \text{at } x = L. \quad (9)$$

A suitable choice of representation uses the new unknown ζ such that

$$\sqrt{\alpha}\zeta + v - \frac{\beta}{Z_c} p = 0.$$

Then the energy balance is:

$$\frac{d\mathcal{E}_{\text{rad}}}{dt} = pv - \frac{\beta}{Z_c} p^2, \quad \text{where} \quad \mathcal{E}_{\text{rad}} = \frac{Z_c}{2}\zeta^2. \quad (10)$$

This representation makes possible the use of time-varying coefficients $\alpha(t), \beta(t)$, e.g. for continuous opening and closing of tone holes.

2.4 Three-way junctions

A tone hole is represented using a three-way junction between the main bore of the instrument, and a smaller tube representing the chimney. The junction model used is that of [6, sec. 7.7], in which flow conservation is enforced, but a pressure discontinuity is introduced through the use of effective acoustic masses. Let p_1, p_2, p_3 denote the pressure values at the three ports of the junction, and v_1, v_2, v_3 the flow entering the junction through each port:

$$v_1 + v_2 + v_3 = 0, \quad (11)$$

$$\begin{pmatrix} p_1 - p_3 \\ p_2 - p_3 \end{pmatrix} = \begin{pmatrix} m_{11} & m_{12} \\ m_{21} & m_{22} \end{pmatrix} \frac{d}{dt} \begin{pmatrix} v_1 \\ v_2 \end{pmatrix}. \quad (12)$$

The energy stored in the junction can be expressed according to the quadratic form defined by the acoustic mass matrix. Thus, as long as the eigenvalues m_s, m_a of the acoustic mass matrix are positive, the model is usable in the time domain, and induces perfect energy conservation through the junction. However measured data of real tonholes configurations lead to negative values for m_a [9]. For our purposes, this is deplorable, as it may lead to instability and divergence. Further research could be devoted to finding a more appropriate formulation ; in the meantime we have chosen to change the second mass for a small, positive value.

2.5 Lumped reed model

We use a reed model with a single degree of freedom y representing the reed opening [4, 6]:

$$\ddot{y} + g\dot{y} + \omega_0^2(y - y_0) = -\frac{S_r \Delta p}{M_r}, \tag{13}$$

where g is a damping factor, ω_0 is a natural frequency of the reed, y_0 is the opening at rest, S_r and M_r model respectively a characteristic surface and characteristic mass of the reed, and $\Delta p = p_m - p(0,t)$ is the pressure difference between the mouth and the beginning of the instrument bore. The mouth pressure p_m may be time-varying. The flow entering the mouthpiece chamber is then given by applying a Bernoulli law. We compensate it with the chamber size variation caused by the motion of the reed.

$$v(0,t) = w y^+ \sqrt{\frac{2|\Delta p|}{\rho}} \mathrm{sign}(\Delta p) - S_r \dot{y}. \tag{14}$$

This model is subject to the following energy balance:

$$\frac{d\mathcal{E}_{\text{reed}}}{dt} = -v(0,t)p(0,t) - Q_{\text{reed}} + \mathcal{S}_{\text{musician}}, \tag{15}$$

$$\text{where} \quad \mathcal{E}_{\text{reed}} = F(y) + \frac{M_r}{2}\dot{y}^2, \tag{16}$$

$$Q_{\text{reed}}(t) = M_r g \dot{y}^2 + w\, y^+ \sqrt{\frac{2}{\rho}}\, |\Delta p|^{3/2}, \tag{17}$$

$$\mathcal{S}_{\text{musician}}(t) = v(0,t)\, p_m(t). \tag{18}$$

The reed's dissipation $Q_{\text{reed}}(t)$ is the sum of mechanical and hydrodynamic effects, and work effected by the musician is represented by $\mathcal{S}_{\text{musician}}(t)$.

2.6 Assembled instrument

All these models can be connected to one another, to form complex instruments with a reed, many toneholes, and many radiating parts. The inner work terms pv then cancel out, resulting in a global energy balance of the form:

$$\frac{d\mathcal{E}_{\text{total}}}{dt} = \mathcal{S}_{\text{musician}}(t) - Q_{\text{total}}(t), \tag{19}$$

where the total energy $\mathcal{E}_{\text{total}}$ is the sum of the energies of each component, and likewise the total dissipated power $Q_{\text{total}}(t)$ is the sum of the power dissipated by each component.

3. NUMERICAL SCHEMES

In order to obtain high-precision solutions of systems formed with the models of instrument parts described previously, one-dimensional finite elements in space are used, followed by an energy-consistent time discretization, in order to ensure numerical stability in the presence of couplings.

3.1 Spatial discretization

Spectral finite elements [10] are used on each section of tubing. The variational formulation of equation (1) is used to find approximate solutions p_h, v_h in a finite-dimensional space composed of piecewise polynomial functions. By using Gauss-Lobatto points as both the interpolation nodes and quadrature points, diagonal mass matrices are obtained. This approach has been shown to be computationally affordable, and to exhibit better results than the Transfer Matrix Method in the frequency domain [6, 10] as soon as viscothermal losses are considered in complex shaped instrument. It is compatible with arbitrary radius profiles, and not just cylinders and cones. Moreover, it allows the straightforward use of non-uniform grids and adaptive high-order elements. The following semi-discrete system is obtained:

$$\begin{cases} M_h^P \dfrac{dP_h}{dt} + B_h^* V_h + \lambda_- E_h^- + \lambda_+ E_h^+ = 0, & \text{(20a)} \\ M_h^V \dfrac{dV_h}{dt} - B_h P_h = 0, & \text{(20b)} \end{cases}$$

where $\lambda_-(t)$, $\lambda_+(t)$ are Lagrange multipliers corresponding to $-v(0,t)$, $v(L,t)$ respectively; diagonal matrices M_h^V and M_h^P are called mass matrices, rectangular matrix B_h corresponds to spatial differentiation, and E_h^- and E_h^+ are vectors containing only zeros and a single one, associated with the first and last degrees of freedom of pressure. System (20) verifies a finite-dimensional analogue of energy balance equation (2).

3.2 Temporal discretization: propagation

For each model, a discrete-time version is sought which preserves a similar energy balance. For acoustic propagation, integration of system (20) is performed with a classical leap-frog scheme, where P_h^n is defined at integer steps and $V_n^{n+1/2}$ is defined on an interleaved grid:

$$\begin{cases} M_h^P \dfrac{P_h^{n+1} - P_h^n}{\Delta t} + B_h^* V_h^{n+1/2} & \text{(21a)} \\ \qquad\qquad + \lambda_-^{n+1/2} E_h^- + \lambda_+^{n+1/2} E_h^+ = 0, \\ M_h^V \dfrac{V_h^{n+3/2} - V_h^{n+1/2}}{\Delta t} - B_h P_h^{n+1} = 0. & \text{(21b)} \end{cases}$$

Assuming the Lagrangian multipliers are known, these equations allow to update P_h^{n+1} and $V_h^{n+3/2}$ alternately. Note that the mass matrices are diagonal, and thus no matrix inversion is required. A discrete energy balance is ob-

tained:

$$\mathcal{E}_h^n = \frac{1}{2}(\bar{V}_h^n)^* M_h^V \bar{V}_h^n + \frac{1}{2}(P_h^n)^* \widetilde{M}_h^P P_h^n, \tag{22}$$

$$\frac{\mathcal{E}_h^{n+1} - \mathcal{E}_h^n}{\Delta t} = -\left(\lambda_-^{n+1/2} E_h^- + \lambda_+^{n+1/2} E_h^+\right)^* \bar{P}_h^{n+1/2}, \tag{23}$$

where the averaged flow and pressure

$$\bar{V}_h^n = \frac{V_h^{n+1/2} + V_h^{n-1/2}}{2},\ \bar{P}_h^{n+1/2} = \frac{P_h^{n+1} + P_h^n}{2}$$

are involved respectively in the energy and the work ; and the modified mass matrix $\widetilde{M}_h^P$ is:

$$\widetilde{M}_h^P = M_h^p - \frac{\Delta t^2}{4} B_h^* M_h^V B_h. \tag{24}$$

Positivity of the energy is required; this leads to the following CFL-stability condition:

$$\Delta t \leq 2 \left[\rho \left((M_h^P)^{-1} B_h^* (M_h^V)^{-1} B_h\right)\right]^{-1/2}. \tag{25}$$

In the presence of viscothermal losses, a similar numerical scheme may be used, with the same stability condition [8].

3.3 Temporal discretization: radiation, junction, reed

Proper numerical schemes must be designed for radiation, junctions and reed to ensure the preservation of a discrete energy, with exact cancellation of the discrete work terms. The following scheme is chosen for radiation:

$$\begin{cases} Z_c \dfrac{\zeta^{n+1} - \zeta^n}{\Delta t} + \sqrt{\alpha}\, E_h^* \bar{P}_h^{n+1/2} = 0, & \text{(26a)} \\ \lambda^{n+1/2} + \sqrt{\alpha}\, \dfrac{\zeta^{n+1} + \zeta^n}{2} - \dfrac{\beta}{Z_c} E_h^* \bar{P}_h^{n+1/2} = 0, & \text{(26b)} \end{cases}$$

where the energy-storing unknown ζ is discretized at integer time steps, and the flow unknown λ is interleaved. With knowledge of P_h^n and $V_h^{n+1/2}$, the update of this scheme is an explicit operation. Indeed, equation (21a) induces an affine relation between two unknowns of this system, namely the discrete tube-end pressure $E_h^* \bar{P}_h^{n+1/2}$ and flow $\lambda^{n+1/2}$. It is thus possible to eliminate the former from system (26) ; a linear system of two equations in two unknowns $(\lambda^{n+1/2}, \zeta^{n+1})$ is obtained, which can be solved algebraically to obtain explicit update formulae. The resulting discrete energy balance is:

$$\mathcal{E}_{\text{rad}}^n = \frac{Z_c}{2}(\zeta^n)^2 \tag{27}$$

$$\frac{\mathcal{E}_{\text{rad}}^{n+1} - \mathcal{E}_{\text{rad}}^n}{\Delta t} = \lambda^{n+1/2}\, E_h^* \bar{P}_h^{n+1/2} - \frac{\beta}{Z_c}\left(E_h^* \bar{P}_h^{n+1/2}\right)^2. \tag{28}$$

Note that this energy balance is a discrete analogue of (10), and that the discrete work term exactly compensates its counterpart in the pipe's energy balance (23).

Time discretizations of junction and reed are done using other energy-consistent schemes. Similarly, their update is performed before the pressure update (21a), but with knowledge of the affine relation between $E_h^* \bar{P}_h^{n+1/2}$ and Lagrange multiplier $\lambda^{n+1/2}$. This approach makes all updates fully explicit. Moreover, the discrete energy balance exactly compensates the work terms in (23), leading to the following global energy balance:

$$\frac{\mathcal{E}_{\text{total}}^{n+1} - \mathcal{E}_{\text{total}}^n}{\Delta t} = \mathcal{S}_{\text{musician}}^{n+1/2} - Q_{\text{total}}^{n+1/2}, \tag{29}$$

which is a discrete version of (19).

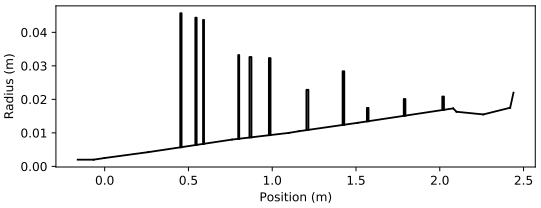

Figure 1. Geometry of the Buffet-Crampon bassoon from [11]. Hole chimneys are placed at their point of junction with the main bore.

4. APPLICATION: SIMULATION OF A BASSOON

The methods described above are applied to simulate a French Buffet-Crampon bassoon, of which the geometry can be found in [11]. The function $R(x)$ describing its radius along the bore axis is affine by parts ; note however that thanks to the 1D finite elements discretization, any bore shape could be used, such as power functions or splines. The overall shape of the bassoon, along with the position of its main holes can be seen in figure 1.

The experiments are performed with the fingering of note C3, i.e. the three holes closest to the reed are closed, which we simulate by setting a boundary condition $v = 0$ at the end of the chimneys. The `frequential` module of OpenWInD, which solves a Fourier-domain version of the instrument's equations, can compute the impedance curve of the bassoon in this setting ; it is displayed in figure 2. More details on this module can be found in [10, 12].

The choice of the reed parameters is challenging, and influences greatly the instrument behavior [3, 13] ; the simulations are performed with the following reed parameters :

$$M_r = 2.04 \times 10^{-3}\,\text{kg}, \quad \omega_0 = 2\pi \times 415\,\text{rad}\,\text{s}^{-1}, \tag{30}$$

$$g = 1.04 \times 10^{3}\,\text{s}^{-1}, \quad y_0 = 3.03 \times 10^{-4}\,\text{m}, \tag{31}$$

$$W = 1.5 \times 10^{-2}\,\text{m}, \quad S_r = 3.0 \times 10^{-4}\,\text{m}^2. \tag{32}$$

The simulations are done on a mesh composed of finite elements of order ranging between 1 and 10 (where elements of order 1 correspond to very short hole chimneys), and length ranging between $4\,\text{mm}$ and $16\,\text{cm}$. The mesh is such that there is always at least one degree of freedom per $1.7\,\text{cm}$, which roughly corresponds to one half-wavelength at $10\,\text{kHz}$. The time step is $\Delta t = 1 \times 10^{-5}\,\text{s}$. In a first simulation, mouth pressure $p_m(t)$ is set to be linearly increasing for $0 < t < 0.01\,\text{s}$, and constant at $5187\,\text{Pa}$ after

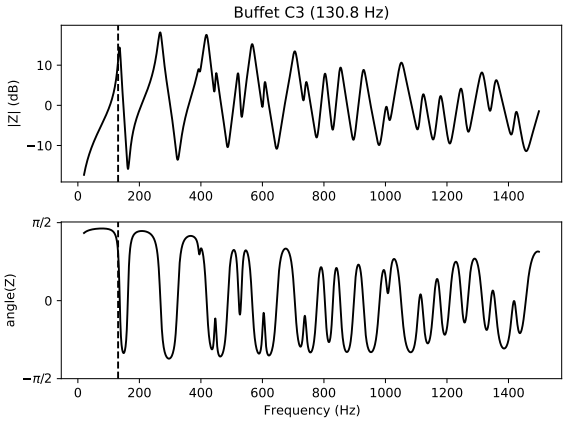

Figure 2. Impedance of the Buffet-Crampon bassoon fingering note C3. Calculated with the `frequential` module of OpenWInD. The vertical dashed line indicates the theoretical playing frequency $130.8\,\mathrm{Hz}$, which is slightly lower than the first peak.

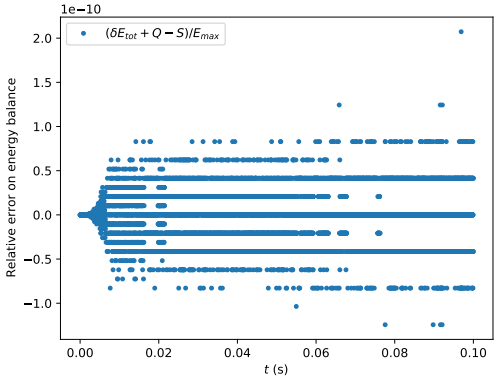

Figure 3. Error on the global energy balance (19) during the simulation.

that. Figure 3 shows the relative error on the global energy balance (19) during the simulation: as expected, the numerical error is only due to the limits of floating-point precision. In a second simulation, a more realistic attack-sustain-release envelope is used for $p_m(t)$, with a maximal pressure of $5706\,\mathrm{Pa}$. The evolution of pressure at the bell of the instrument is displayed in figure 4. Periodic oscillation is visible. Pressure and flow are also available everywhere along the bore, as well as in each hole. Sound examples will be played during the presentation.

5. CONCLUSION AND PROSPECTS

A high-precision time-domain simulation method for wind instruments has been presented. The classical equations of acoustic propagation in a variable section pipe are used, optionally with viscothermal losses, and discretized in space using 1D high-order finite elements. Models of radiation impedance, tone holes, and reed close the acoustical system ; special care is taken to ensure all models verify an energy balance. Finite differences are used for

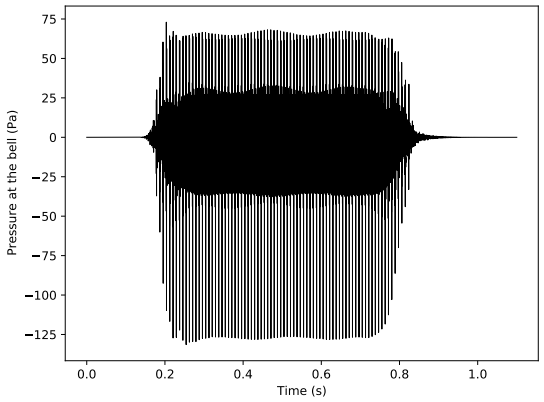

Figure 4. Evolution of the bell pressure of a Buffet-Crampon bassoon playing note C3.

the time discretization, ensuring numerical stability via energy techniques. These methods can be applied to simulate complex real instruments. An open-source Python implementation of the methods is available on the OpenWInD project website [1]. It provides a reliable foundation on which additional state-of-the-art models may be combined.

6. REFERENCES

[1] J. Chabassier, G. Castera, A. Ernoult, A. Thibault, and R. Tournemenne, "Open wind instrument design - a python toolbox assisting instrument makers." `https://openwind.gitlabpages.inria.fr/web/`, 2020.

[2] G. P. Scavone, An acoustic analysis of single-reed woodwind instruments with an emphasis on design and performance issues and digital waveguide modeling techniques. PhD thesis, Citeseer, 1997.

[3] P.-A. Taillard, F. Silva, P. Guillemain, and J. Kergomard, "Modal analysis of the input impedance of wind instruments. application to the sound synthesis of a clarinet," Applied acoustics, vol. 141, pp. 271–280, 2018.

[4] S. Bilbao, "Direct simulation of reed wind instruments," Computer Music Journal, vol. 33, no. 4, pp. 43–55, 2009.

[5] S. W. Rienstra, "Webster's horn equation revisited," SIAM Journal on Applied Mathematics, vol. 65, no. 6, pp. 1981–2004, 2005.

[6] A. Chaigne and J. Kergomard, Acoustics of musical instruments. Springer, 2016.

[7] S. Bilbao and R. Harrison, "Passive time-domain numerical models of viscothermal wave propagation in acoustic tubes of variable cross section," The Journal of the Acoustical Society of America, vol. 140, no. 1, pp. 728–740, 2016.

[8] A. Thibault and J. Chabassier, "Dissipative time-domain 1d model for viscothermal acoustic propagation in wind instruments," [Manuscript submitted for publication], 2020.

[9] V. Dubos, J. Kergomard, A. Khettabi, J.-P. Dalmont, D. Keefe, and C. Nederveen, "Theory of sound propagation in a duct with a branched tube using modal decomposition," Acta Acustica united with Acustica, vol. 85, no. 2, pp. 153–169, 1999.

[10] R. Tournemenne and J. Chabassier, "A comparison of a one-dimensional finite element method and the transfer matrix method for the computation of wind music instrument impedance," Acta Acustica united with Acustica, vol. 105, no. 5, pp. 838–849, 2019.

[11] J. Kergomard and J.-M. Heinrich, "Le basson : historique, fabrication, acoustique. l'anche double : fabrication, botanique, le grattage.," Bulletin du Groupe d'Acoustique Musicale, vol. 82-83, 1975.

[12] J. Chabassier, A. Ernoult, O. Geber, A. Humeau, A. Thibault, R. Tournemenne, and T. van Baarsel, "The virtual workshop openwind : a python toolbox assisting wind instrument makers.," in Forum Acusticum, (Paris), Dec. 2020.

[13] F. Silva, J. Kergomard, C. Vergez, and J. Gilbert, "Interaction of reed and acoustic resonator in clarinet-like systems," The Journal of the Acoustical Society of America, vol. 124, no. 5, pp. 3284–3295, 2008.